Tian et al. Nanoscale Research Letters 2013, 8:203
http://www.nanoscalereslett.com/content/8/1/203

Nanoscale Research Letters
a SpringerOpen Journal

NANO EXPRESS Open Access

First-principles investigation on the segregation of Pd at $LaFe_{1-x}Pd_xO_{3-y}$ surfaces

Zhi-xue Tian[1], Akifumi Uozumi[2], Ikutaro Hamada[3], Susumu Yanagisawa[4], Hidetoshi Kizaki[1], Kouji Inagaki[1] and Yoshitada Morikawa[1,5*]

Abstract

First-principles calculations were performed to investigate the effect of Pd concentration and oxygen vacancies on the stability of Pd at $LaFeO_3$ surfaces. We found a much stronger tendency of Pd to segregate by taking the aggregation of Pd at $LaFe_{1-x}Pd_xO_{3-y}$ surfaces into consideration, resulting in a pair of Pd-Pd around a vacancy. Moreover, we predicted that one oxygen-vacancy-containing FeO_2-terminated surfaces would be stable at high temperatures by comparing the stability of $LaFe_{1-x}Pd_xO_{3-y}$ surfaces, which further supports our previous conclusion that a Pd-containing perovskite catalyst should be calcined at 1,073 K or higher temperatures in air to enhance the segregation of Pd in the vicinity of surfaces to rapidly transform the Pd catalyst from oxidized to reduced states on the perovskite support.

Keywords: Perovskite, $LaFeO_3$, Palladium, Density functional theory, Surface segregation

Background

A three-way catalyst simultaneously transforms toxic exhaust emissions from motor vehicles into harmless gases. However, the sintering problem, i.e., the growth and agglomeration of precious metal particles on conventional catalysts during vehicle use dramatically degrades catalytic activity, and large amounts of precious metals are required to retain the activity of catalysts after long periods of use. Thus, intelligent catalysts have attracted worldwide attention due to their greatly improved durability as a result of the self-regenerative function of precious metal nanoparticles [1-3]. It has been confirmed that the activity of catalysts can be preserved, and the amount of precious metals that are required can be reduced by 70% to 90% [4,5]. The self-regenerative function, which can be explained as resulting from the transformation of the state of precious metals (Pd, Pt, and Rh) that reversibly move into and out of the $LaFe_{1-x}M_xO_3$ perovskite lattice, significantly suppresses the growth of precious metals during the use of catalysts.

Thus far, many experiments have been devoted to research on the state of Pd in perovskite in redox processes. Uenishi et al. [6] investigated the superior start-up activity of $LaFePdO_x$ at low temperatures (from 100°C to 400°C) using X-ray spectroscopic techniques under the practical conditions where they controlled automotive emissions. They found the Pd^0 phase partially segregated outside the surface even at low temperatures; thus, the segregation of Pd^0 under a reductive atmosphere induced the start-up activity of $LaFePdO_x$. Eyssler et al. found a high concentration of Pd distributed on the $LaFeO_3$ (LFO) surface that contributed to high methane combustion due to the formation of PdO in which Pd^{2+} was in square planar coordination. Additionally, two Pd species (Pd^{2+} at the surface and Pd^{3+} in a solid solution) were found to be generated in further calcination. Pd^{2+} and Pd^{3+} could be transformed in equilibrium under thermal treatment conditions [7,8]. More recently, Eyssler et al. studied the state of Pd in different B-site substitutions and compared the effect of catalytic activities on methane combustion. A well-dispersed octahedral Pd-O species was found for Fe- and Co B- site cations, and PdO particles were on the $LaMnO_3$ surface [9]. Above all, related investigations have become more important as the activity of

---

* Correspondence: morikawa@prec.eng.osaka-u.ac.jp
[1] Division of Precision Science & Technology and Applied Physics, Graduate School of Engineering, Osaka University, 2-1, Yamada-okaSuita, Osaka 565-0871, Japan
[5] Elements Strategy Initiative for Catalysts and Batteries (ESICB), Kyoto University, Katsura, Kyoto 615-8520, Japan
Full list of author information is available at the end of the article

catalysts strongly depends on the state of the precipitated Pd.

Hamada et al. [10] more recently found in a density functional theory (DFT) investigation that oxygen vacancies (V_Os) that formed near the LFO surface promoted the segregation of Pd. They also proposed a scenario that perovskite containing precious metal is calcined during the catalyst preparation step at 1,073 K for 2 h in air, and then V_Os are produced that enhance Pd segregation, resulting in a $LaPdO_{3-y}$ layer that eventually forms close to the surface. The $LaPdO_{3-y}$ layer in the vicinity of the surface promotes efficient switching between Pd metal particles under reductive conditions and the dissolved state of Pd in the $LaFe_{1-x}Pd_xO_3$ perovskite lattice under oxidative conditions. Therefore, the $LaPdO_{3-y}$ layers formed in the vicinity of the oxide surface play a key role in the self-regenerative function. Almost simultaneously, transmission electron microscopy observations [11] of atomic-scale processes in Pd-LFO catalysts have demonstrated that redox reactions between the formation of Pd particles on the Pd-LFO surface under reducing conditions and the dissolution of Pd particles into LFO under oxidizing conditions take place in spatially-limited areas, especially in the proximity of oxide surfaces, indicating strong interactions between Pd and oxide surfaces. Katz's results also provided strong support for the mechanism proposed by Hamada et al. However, the stability of the $LaPdO_{3-y}$ layer and the mechanism for Pd leaving the $LaPdO_{3-y}$ layer have not been discussed in detail. The interaction between Pd atoms in the perovskite host is especially important considering the possibility of nanoscale spinodal decomposition as pointed out by Kizaki et al. [12]. Therefore, we systemically studied the relative stability of the Pd_mV_{On}-containing surfaces (m =1 and 2 and n =0, 1, and 2) in our present work to investigate possible phases appearing in steps to prepare catalysts at high temperature in air.

Methods

Model and computation

We have calculated the lattice constants [13] of LFO and the segregation tendency of Pd at two terminations of the perovskite surfaces with and without V_O by using state [14,15] and quantum ESPRESSO (QE) [16] codes. We found that both state and QE codes yielded the similar bulk lattice constants and caused the segregation behavior of Pd, which was a strong indication that both codes could admirably describe the properties of Pd incorporated in the $LaFe_{1-x}Pd_xO_{3-y}$ surfaces. Here, we employed the state code to do the first-principles calculations. The ion-electron interactions were described using ultrasoft pseudopotentials [17], and the exchange and correlation potential was represented by a generalized gradient approximation (GGA) in the Perdew-Burke-Ernzerhof formula [18]. DFT calculations with Hubbard correction (DFT+U) are known to correct the bandgap and magnetic moment in local-density approximation and generalized gradient approximation calculations. This method can yield reasonable agreement with the experimental results. We omitted DFT+U from this work because Hamada et al. verified [10] that electronic structures with DFT+U are qualitatively the same as those in GGA calculations, and they have not changed their conclusions. However, since the relative energies that are used to determine the stability of perovskite surfaces might be influenced by the exchange and correlation potential, even though DFT+U fails to give better results than GGA calculations to predict the phase stability of hematite surfaces [19], we still intend to investigate the effect of DFT+U in later work. The original unit cell used to construct the LFO perovskite surface was a $GdFeO_3$-type orthorhombic unit cell (adapted from Figure one in [13]), in which the local magnetic moments of Fe are aligned in G-type anti-ferromagnetic order. The relaxed lattice constants for a, b, and c in bulk LFO correspond to 0.575, 0.559, and 0.792 nm, respectively, which are in reasonable agreement with the experimental values [20] of 0.558, 0.556, and 0.785 nm. The cutoff energies for the wave function and augmentation charge density are 25 Ry for the former and 225 Ry for the latter.

We modeled the $\sqrt{2} \times \sqrt{2}$ LFO (001) surface by using a repeated slab model. Hamada et al. [10] had already shown and we confirmed [13] that one V_O formed in the LFO (001) surface promoted the tendency of Pd to segregate in bulk. Moreover, we further demonstrated that Pd has the strongest tendency to segregate at FeO_2-terminated surfaces containing V_Os, in comparison with three other surfaces, i.e., LaO-terminated surfaces with and without V_Os and the perfect FeO_2-terminated surfaces. Additionally, Lee et al. [21] calculated a surface phase diagram of the LFO (010) surface and argued that the LaO-terminated surface could be predicted to be stable at lower temperature (773 K), which was in agreement with the previous experimental results measured by X-ray photoelectron spectra [22,23]. In contrast, the FeO_2-terminated surface became dominant at high temperatures (>1,500 K). Therefore, thermal treatment at high temperature is essential to make FeO_2-terminated surfaces more stable. We thus examined FeO_2-terminated surfaces in this work. The atomic configuration for a pristine FeO_2-terminated surface is in Figure 1, which was obtained with visual molecular dynamics [24]. Our repeated slab model consisted of nine atomic layers, i.e., five FeO_2 layers and four LaO layers. Further, one unit cell contained eight La atoms, 10 Fe atoms, and 28 O atoms in total. Brillouin-zone integration was carried out within a Monkhorst-Pack [25] scheme using a uniform (4 × 4 × 1) mesh. We inserted a vacuum region of 11 Å to minimize the interaction between two adjacent slabs. We fixed the two bottom layers to the bulk coordinates during the geometry optimizations and allowed atomic relaxation for the rest of the layers.

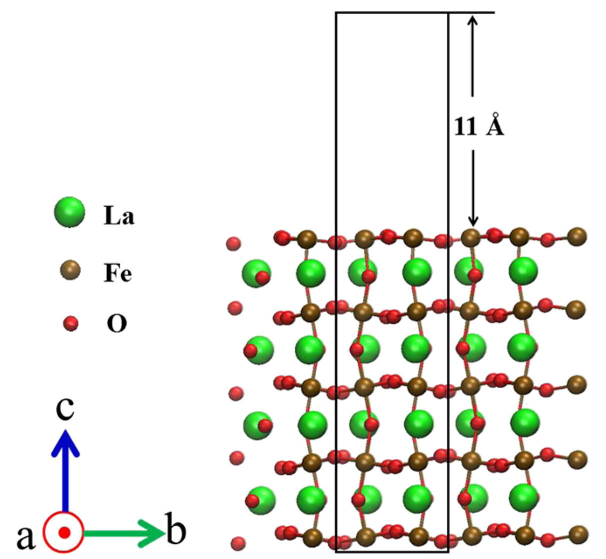

Figure 1 Side views of FeO_2-terminated surfaces. A vacuum region with a thickness of 11 Å is placed above the top surface. The green, brown, and red spheres correspond to La, Fe, and O, respectively. The computational unit cell used in the present research is indicated by the black solid line. The bottom two layers were fixed during optimization.

Results and discussion

Simplified 2D tables that represent the complicated atomic configurations of perovskite surfaces have been provided in Figure 2 to clarify the discussion. Configurations with negative formation energies are more stable than the reference configuration. One Pd segregating from the third FeO_2 layer to the surface just releases an energy of about 0.08 eV [13] (Figure 2 group I (a) and (b)) as we demonstrated without V_Os. However, when one Pd has already segregated on the topmost site of a perfect LFO surface, the additional Pd prefers to stay inside the bulk rather than segregate onto the surface as shown in Figures 2 group I (c) to (e). One first has to determine the positions of V_Os and Pd atoms in studying the effect induced by V_Os on the stability of Pd atoms. We have to calculate all the possible configurations containing V_Os and Pd. Hamada et al. [10] pointed out

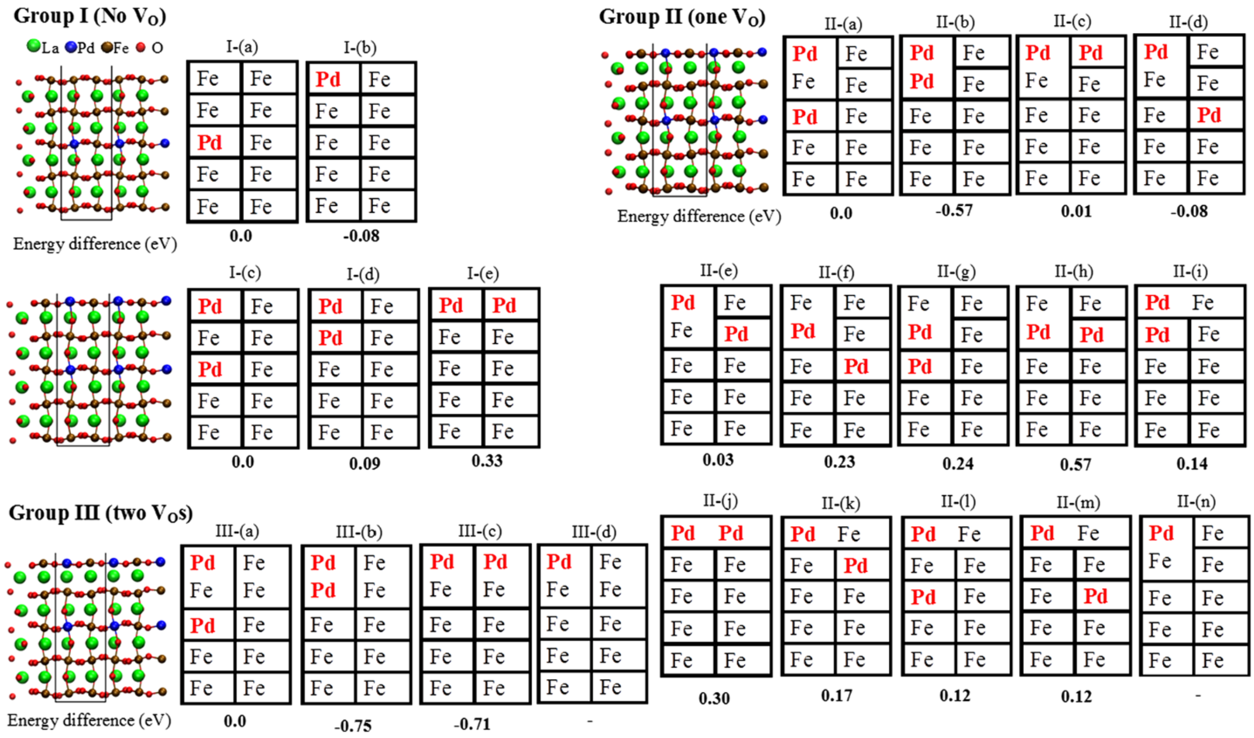

Figure 2 Simplified 2D tables that represent complicated structures of perovskite surfaces containing Pd_n (n=1 and 2). Groups I to III are for the geometries with no V_O, one V_O, and two V_Os, respectively. The atomic configurations for each group, which are schematically represented by the table of panel (**a**), are indicated by the ball and stick model. The uncapping unit cell is indicated by the black line as seen in Figure 1. The rows containing Fe (Pd) in each table represent FeO_2 (PdO_2) layers, and the vertical lines represent O atoms in FeO_2 (PdO_2) layers. The horizontal lines represent O atoms in LaO layers (La atoms are not explicitly shown). The absence of vertical (horizontal) lines means V_O forming at the surface (subsurface) site. The calculated difference in energy (in eV) for each panel relative to the total energy of the surface in panel (a) is also listed.

that the most stable site for V_Os is the topmost surface for pristine LFO and the subsurface (LaO layer) O site for Pd located in the first layer of the LFO surface. We considered V_Os formed at those two possible sites along with various configurations of Pd atoms at the FeO_2-terminated surface. We set the first configuration in panel (a) in group II to the reference state in which one Pd atom was located in the first FeO_2 layer, the second Pd atom was in the third FeO_2 layer, and a V_O was located in the first LaO layer just under the first Pd. The positions of the first Pd atom and V_O were found to have the most stable configuration. Positive formation energies for panels (i) to (m) in group II indicate that V_Os that formed on the topmost surface is unstable. However, the most stable state was found with a formation energy of about -0.57 eV when a V_O was located at the subsurface nearly at the center of two Pd atoms, as seen in Figure 2 group II (b). However, one of the Pd atoms tended to be buried in the second FeO_2 layer (panel (b)) rather than exposed to the vacuum (panel (c) in group II), and the energy discrepancy between panels (b) and (c) was as large as 0.58 eV. We analyzed the projected density of state (PDOS) of the two Pd atoms in the V_O-containing surfaces to understand the origin for the difference in stability between panels group II (b) and (c). All the results are presented in Figure 3. We denoted the Pd located at the top-left site in the unit cell in Figure 2 group II (a) to (c) as Pd-1 and the other one as Pd-2. Where Pd-2 stayed inside the bulk (Figure 2 group II (a)), the PDOS of Pd-1 looked similar to that in Figure five (e) in [13], i.e., a single Pd at the first FeO_2 layer with one V_O beneath it. The V_O beneath Pd-1 reduces hybridization between the Pd d_{3z}^2 state and O p state, leading to significant stabilization of the d_{3z}^2 state. The degenerated e_g states of $4d$-orbitals for Pd-2 are singly occupied (Figure 3a$_2$). When Pd-2 replaces the Fe

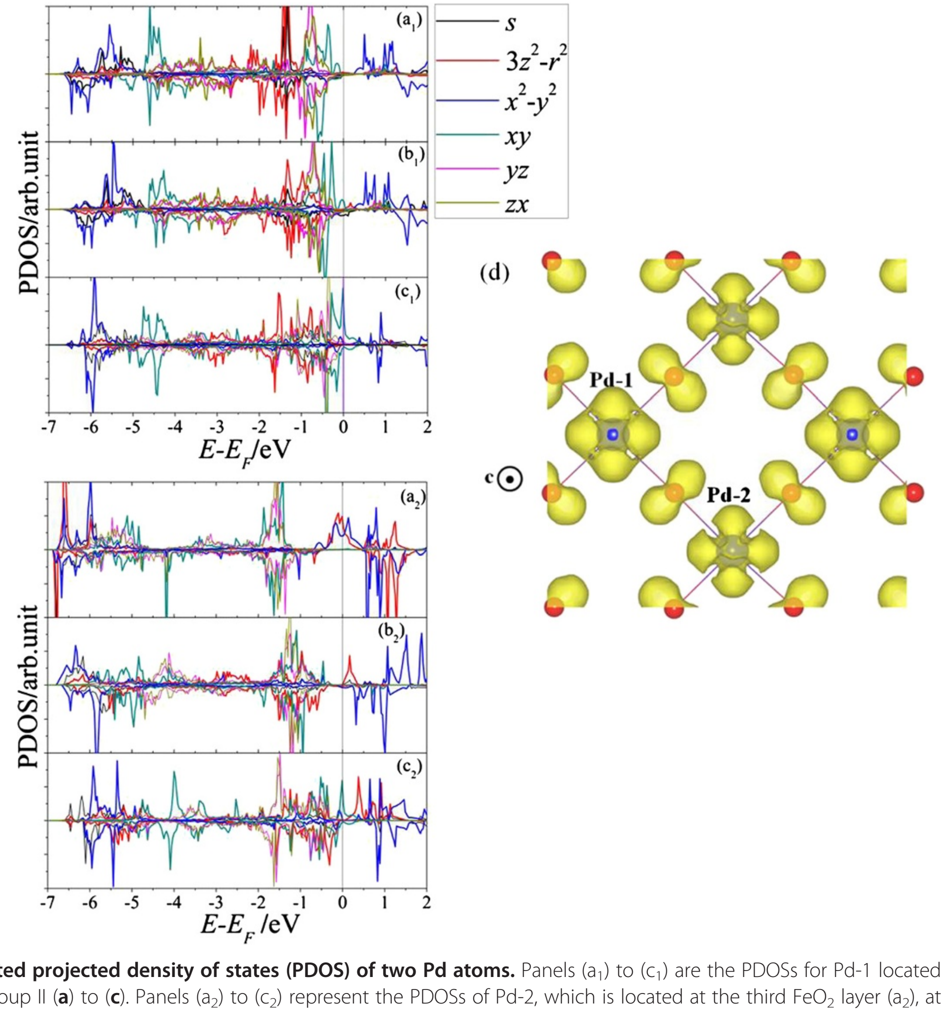

Figure 3 Calculated projected density of states (PDOS) of two Pd atoms. Panels (a$_1$) to (c$_1$) are the PDOSs for Pd-1 located at the top-left site of Figure 2 group II (**a**) to (**c**). Panels (a$_2$) to (c$_2$) represent the PDOSs of Pd-2, which is located at the third FeO_2 layer (a$_2$), at the subsurface (b$_2$), or the first FeO_2 layer (c$_2$). Positive (negative) values refer to spin-up (spin-down) states. The line through the zero point on the horizontal axis represents the Fermi level. (**d**) is the top view of the calculated isosurface of the partial charge density of the PdO_2-terminated surface containing V_O in the spin-up state in an energy window of (-0.1, 0.1) eV. The yellow-curved isosurfaces stand for the charge density of 0.6 a.u.$^{-3}$.

atom at the second FeO_2 layer (Figure 2b), the change in PDOS of Pd-1 seems rather small and similar to that in panel (a_1). However, the degeneracy of the e_g state is lifted for Pd-2 because of the missing apical oxygen atom, leading to a downward shift in d^2_{3z} beneath the Fermi level, except for a small antibonding state near the Fermi level associated with hybridization between the Pd d^2_{3z} and p state of oxygen atom beneath it. The t_{2g} states are also fully occupied in the form of a stable closed shell. The degeneracy of the e_g state is lifted due to the lowering of symmetry at the surface for Pd-2 located at the first FeO_2 layer (Figure 2 group II (c)). However, as there is another O at the subsurface, a much stronger antibonding Pd d^2_{3z} state appears near the Fermi level in contrast to that in panel (b_2). Additionally, the d_{xy} state remarkably increases in energy due to increased hybridization between the Pd-d_{xy} and O-$p_{y/x}$ states, and an especially sharp peak emerges at the Fermi level in the spin-up state. The Pd d_{xy} state also appears near the Fermi level for Pd-1 as shown in panel (c_1). The corresponding partial charge density for the peak at the Fermi level has been drawn on the (001) plane in panel (d). The spin-up partial charge density exhibits strong antibonding states in the form of $pd\pi^*$ bonds between Pd and O in the energy window from -0.1 to +0.1 eV relative to the Fermi energy. As a result, the additional Pd at the neighboring surface site is less stable than that at the second FeO_2 layer.

Since V_Os are more likely to form at the subsurface (LaO layer) than the surface in the Pd-containing FeO_2-terminated surface, we placed another V_O in the same LaO layer (Figure 2 group III (a) to (c)). If two V_Os are both located at the subsurface, the second Pd atom tends to substitute the Fe atom either at the second FeO_2 layer forming a pair of Pd atoms (Figure 2 group III (b)) or on the surface forming the PdO_2 layer (Figure 2 group III (c)). The difference in energy between these two configurations is less than 0.05 eV. Thus, the additional V_O stabilizes the PdO_2-layer exposed to the vacuum.

Thus far, we have assumed the existence of V_O. However, the concentration of V_Os depends on their formation energy. Therefore, we have to verify the stability of surfaces containing V_O(s) with different concentrations of Pd by taking the formation energy of V_Os into account to further strengthen our conclusion. We calculated the relative energies of surfaces containing Pd_mV_{On} (m =1 and 2 and n =0, 1, and 2) relative to the perfect slab (without V_Os) with Pd inside the bulk of LFO (see Figure 2 group I (a)). Note that the systems we have discussed here are surfaces with Pd atom(s) and V_O(s) located on/near the surface. The relative energies (ΔE^{rel}) as a function of the chemical potential of oxygen ($\Delta\mu_O$) are shown in Figure 4. The corresponding geometries for the Pd_mV_{On}-containing surfaces are all included in Figure 2. Since two Pd atoms fail to segregate near/at the surface adjacently without V_Os, the results for the Pd_2-containing perfect surface excluded from Figure 4. The ΔE^{rel} for each colored line is calculated as:

$$\text{Green line}: \Delta E^{\mathrm{rel}} = 2E^{\mathrm{tot}}_{\mathrm{PdFeO_4/(LaO)_2/(FeO_2)_2/(LaFeO_3)_6}} - 2E^{\mathrm{tot}}_{\mathrm{ref}}, \tag{1}$$

$$\text{Green line}: \Delta E^{\mathrm{rel}} = 2E^{\mathrm{tot}}_{\mathrm{PdFeO_4/La_2O_1/(FeO_2)_2/(LaFeO_3)_6}} - 2E^{\mathrm{tot}}_{\mathrm{ref}} + 2\mu_O, \tag{2}$$

$$\text{Pink line}: \Delta E^{\mathrm{rel}} = 2E^{\mathrm{tot}}_{\mathrm{PdFeO_4/La_2/(FeO_2)_2/(LaFeO_3)_6}} - 2E^{\mathrm{tot}}_{\mathrm{ref}} + 4\mu_{\mathrm{O}}, \tag{3}$$

$$\text{Red line}: \Delta E^{\mathrm{rel}} = E^{\mathrm{tot}}_{\mathrm{PdFeO_4/La_2O_1/PdFeO_4/(LaFeO_3)_6}} + E^{\mathrm{tot}}_{\mathrm{(FeO_2)_2/(LaFeO_3)_8}} - 2E^{\mathrm{tot}}_{\mathrm{ref}} + \mu_{\mathrm{O}}, \tag{4}$$

$$\text{Blue line}: \Delta E^{\mathrm{rel}} = E^{\mathrm{tot}}_{\mathrm{PdFeO_4/La_2/PdFeO_4/(LaFeO_3)_6}} + E^{\mathrm{tot}}_{\mathrm{(FeO_2)_2/(LaFeO_3)_8}} - 2E^{\mathrm{tot}}_{\mathrm{ref}} + 2\mu_{\mathrm{O}}, \tag{5}$$

where the first items in Equations 1 to 5 on the right-hand side are the total energies of the Pd_mV_{On}-containing (m =1 and 2 and n =0, 1, and 2) surfaces, with their subscripts describing their compositions. E^{tot}_{ref}

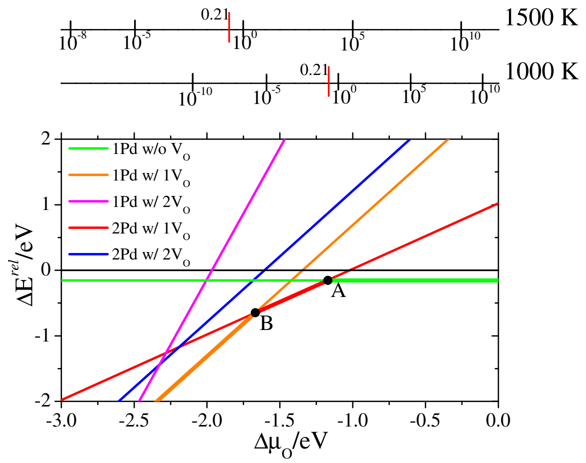

Figure 4 Calculated relative energies of five LFO surfaces containing Pd_mV_{On}. This is with respect to the dissolution phase of the $LaFe_{1-x}Pd_xO_3$ slab as a function of $\Delta\mu_O$ and oxygen partial pressure at high temperatures.

represents the total energy of the reference surface that contains one solid-solution state of Pd inside the bulk. The $E^{\mathrm{tot}}_{(\mathrm{FeO_2})_2/(\mathrm{LaFeO_3})_8}$ in Equations 4 and 5 is the total energy of the pristine FeO_2-terminated surface. The μ_O is the chemical potential of oxygen. The chemical potentials of oxygen in the LFO bulk and gas phase are equal under equilibrium conditions. The μ_O based on an ideal gas approximation is directly connected with the partial pressure (p (O_2)) and temperature (T) by

$$\mu^{\mathrm{gas}}_{O_2}(T,p) = \mu^{\mathrm{gas}}_{O_2}(T,p^0) + kT\ln\left(\frac{p}{p^{\mathrm{o}}}\right), \tag{6}$$

$$\begin{aligned}\Delta\mu^{\mathrm{gas}}_{O}(T,p) &= \frac{1}{2}\left(\mu^{\mathrm{gas}}_{O_2}(T,p) - E^{\mathrm{gas}}_{O_2}\right)\\ &= \Delta\mu^{\mathrm{gas}}_{O}(T,p^0) + \frac{1}{2}kT\ln\left(\frac{p}{p^{\mathrm{o}}}\right),\end{aligned} \tag{7}$$

in which k is the Boltzmann constant and p^0 is taken to be the standard pressure. $\mu^{gas}_{O_2}$ is the total energy of an isolated O_2 molecule. The $\Delta\mu^{gas}_{O}(T,p^0)$ item is determined by using thermodynamic data from the thermochemical tables [26]. Hence, we can obtain the formation energy of V_O(s) based on Equations 2 to 5 by subtracting the item in Equation 1. As we assumed that the chemical potential of La would be very low in the present research, no metallic La or La oxides could precipitate on the surface although the La-O bonds were broken due to the formation of V_Os in the first LaO layer (Figures 2 groups II and III). According to the equations, the positive ΔE^{rel} means the reference surface is more stable.

We can find from Figure 4 that when $\Delta\mu_O$ is greater than -1.17 eV (point A), no V_Os form on the surface. The Pd-segregated surface (Figure 2 group I (b)) is slightly more stable than the surface with Pd inside the bulk of the perovskite (Figure 2 group I (a)). This indicates that Pd preferentially stays at the first layer of the LFO surface than the bulk position to some extent. One V_O in the surface appears at the subsurface (LaO layer) when $\Delta\mu_O$ is lower than -1.17 eV. The surface containing Pd_2V_O is predicted to be stable between points A and B, indicating conditions with standard pressure at temperatures between 1,000 and 1,500 K. Two Pd atoms attract each other in such a surface by sharing one V_O in the first LaO layer (Figure 2 group II (b)). The Pd_1V_{O1}-containing surface (Figure 2 group II (n)) becomes dominant at $\Delta\mu_O$ below -1.67 eV (point B) under standard pressure at temperatures over 1,500 K. Two V_Os-containing surfaces are predicted to be dramatically unstable compared with the other three surfaces due to the greater formation energy of two V_Os under the conditions given in Figure 4. The Pd_1V_{O2}-containing surface (Figure 2 group III (d)) will appear under standard pressure at temperatures far above 1,500 K (the pink line: the critical point is beyond the scale of Figure 4). The surface containing Pd_2V_{O2} (Figure 2 group III (b)) for the blue line is predicted to be unstable under any conditions as presented in Figure 4. From what we have mentioned above, one V_O can be produced at the first LaO layer of the FeO_2-terminated surfaces with segregated Pd_m (m =1 and 2) under reasonable working conditions, and such surfaces are predicted to be dominantly stable over a wide range of $\Delta\mu_O$.

Conclusions

We investigated what effect oxygen vacancies had on the tendency of additional Pd atoms to segregate at the $LaFe_{1-x}Pd_xO_{3-y}$ surface, as well as compared the relative stability of FeO_2-terminated surfaces that contained Pd_mV_{On} versus the oxygen chemical potential, by using first-principles theoretical calculations. We pointed out that Pd atoms repulse one another without V_Os. However, if there are V_Os at the subsurface layer, Pd atoms become attractive, forming a pair of Pd atoms while sharing one V_O. Furthermore, we clarified that the FeO_2-terminated surface containing Pd_mV_O could be predicted to become stable over a wide range of oxygen chemical potentials below -1.17 eV. Therefore, the present results provide support that the calcination of precious metals containing catalysts at 1,073 K or high temperatures in air during the catalyst preparation step leads to the formation of oxygen vacancies near the surface and then enhances the formation of a $LaPdO_{3-y}$ layer in the vicinity of the $LaFeO_3$ oxide surface.

Competing interests

The authors declare that they have no competing interests.

Authors' contributions

ZT, AU, IH, and SY carried out calculations with the help of HK and KI and drafted the manuscript. YM participated in the design of the study and helped to draft the manuscript. All authors read and approved the final manuscript.

Acknowledgments

The present work was partly supported by a Ministry of Education, Culture, Sports, Science and Technology (MEXT) program called the "Elements Strategy Initiative to Form Core Research Center" (since 2012). The Advanced Institute for Materials Research (AIMR) was established by the World Premier Research Center Initiative (WPI), MEXT, Japan. The calculations were done at the supercomputer centers of Osaka University, the Institute for Solid State Physics, the University of Tokyo, and Tohoku University.

Author details

[1]Division of Precision Science & Technology and Applied Physics, Graduate School of Engineering, Osaka University, 2-1, Yamada-okaSuita, Osaka 565-0871, Japan. [2]Insitute of Scientific and Industrial Research, Osaka University, 8-1 Mihogaokalbaraki, Osaka 567-0047, Japan. [3]Advanced Institute for Materials Research (AIMR), Tohoku University, Sendai 980-8577, Japan. [4]Department of Physics and Earth Science, Faculty of Science, University of the Ryukyus, 1 SenbaruNishihara, Okinawa 903-0213, Japan. [5]Elements Strategy Initiative for Catalysts and Batteries (ESICB), Kyoto University, Katsura, Kyoto 615-8520, Japan.

Received: 31 December 2012 Accepted: 21 March 2013
Published: 1 May 2013

References

1. Nishihata Y, Mizuki J, Akao T, Tanaka H, Uenishi M, Kimura M, Okamoto T, Hamada N: Self-regeneration of a Pd-perovskite catalyst for automotive emissions control. *Nature* 2002, **418**:164–167.
2. Tanaka H, Uenishi M, Taniguchi M, Tan I, Narita K, Kimura M, Kaneko K, Nishihata Y, Mizuki J: The intelligent catalyst having the self-regenerative function of Pd, Rh and Pt for automotive emissions control. *Catal Today* 2006, **117**:321–328.
3. Tanaka H, Taniguchi M, Uenishi M, Kajita N, Tan I, Nishihata Y, Mizuki J, Narita K, Kimura M, Kaneko K: Self-regenerating Rh- and Pt-based perovskite catalysts for automotive-emissions control. *Angew Chem Int Ed* 2006, **45**:5998–6002.
4. Sato N, Tanaka H, Tan I, Uenishi M, Kajita N, Taniguchi M, Narita K, Kimura M: Research on the co-free intelligent catalyst. In *Proceedings of the SAE 2003 World Congress & Exhibition: March 3, 2003*. Detroit. Warrendale: SAE International; 2003.
5. Tanaka H, Taniguchi M, Kajita N, Uenishi M, Tan I, Sato N, Narita K, Kimura M: Design of the intelligent catalyst for Japan ULEV standard. *Topics Catal* 2004, **30/31**:389.
6. Uenishi M, Taniguchi M, Tanaka H, Kimura M, Nishihata Y, Mizuki J, Kobayashi T: Redox behavior of palladium at start-up in the perovskite-type LaFePdO*x* automotive catalysts showing a self-regenerative function. *Appl Catal Environ* 2005, **57**:267–273.
7. Eyssler A, Mandaliev P, Winkler A, Hug P, Safonova O, Figi R, Weidenkaff A, Ferri D: The effect of the state of Pd on methane combustion in Pd-doped LaFeO$_3$. *J Phys Chem C* 2010, **114**:4584.
8. Eyssler A, Winkler A, Mandaliev P, Hug P, Weidenkaff A, Ferri D: Influence of thermally induced structural changes of 2 wt% Pd/LaFeO$_3$ on methane combustion activity. *Appl. Catal. B: Enviro.* 2011, **106**:494–502.
9. Eyssler A, Winkler A, Nachtegaal M, Matam SK, Hug P, Safonova O, Weidenkaff A, Ferri D: On the state of Pd in Perovskite-type oxidation catalysts of composition A(B, Pd)O3±δ (A = La, Y; B = Mn, Fe, Co). *Chem Mater* 2012, **24**:1864–1875.
10. Hamada I, Uozumi A, Morikawa Y, Yanase A, Katayama-Yoshida H: A density functional theory study of self-regenerating catalysts LaFe$_{1-x}$M$_x$O$_{3-y}$ (M = Pd, Rh, Pt). *J Am Chem Soc* 2011, **133**:18506–18509.
11. Katz M, Graham G, Duan Y, Liu H, Adamo C, Schlom D, Pan X: Self-regeneration of Pd–LaFeO$_3$ catalysts: new insight from atomic-resolution electron microscopy. *J Am Chem Soc* 2011, **133**:18090–18093.
12. Kizaki H, Kusakabe K, Nogami S, Katayama-Yoshida H: Generation of nano-catalyst particles by spinodal nano-decomposition in perovskite. *Appl Phys Express* 2008, **1**:104001.
13. Tian ZX, Inagaki K, Morikawa Y: Density functional theory on the comparison of the Pd segregation behavior at LaO- and FeO$_2$-terminated surfaces of LaFe$_{1\text{-}x}$Pd$_x$O$_{3\text{-}y}$. *Current Appl Phys* 2012, **12**:S105.
14. Morikawa Y, Ishii H, Seki K: Theoretical study of *n*-alkane adsorption on metal surfaces. *Phys Rev B* 2004, **69**:041403.
15. Sawada H, Morikawa Y, Terakura K, Hamada N: Jahn-Teller distortion and magnetic structures in LaMnO$_3$. *Phys Rev B* 1997, **56**:12154–12160.
16. Giannozzi P, Baroni S, Bonini N, Calandra M, Car R, Cavazzoni C, Ceresoli D, Chiarotti GL, Cococcioni M, Dabo I, Corso AD, Gironcoli S, de Fabris S, Fratesi G, Gebauer R, Gerstmann U, Gougoussis C, Kokalj A, Lazzeri M, Martin-Samos L, Marzari N, Mauri F, Mazzarello R, Paolini S, Pasquarello A, Paulatto L, Sbraccia C, Scandolo S, Sclauzero G, Seitsonen AP, Smogunov A, Umari P, Wentzcovitch RM: QUANTUM ESPRESSO: a modular and open-source software project for quantum simulations of materials. *J Phys Condens Matter* 2009, **21**:395502.
17. Vanderbilt D: Soft self-consistent pseudopotentials in a generalized eigenvalue formalism. *Phys Rev B* 1990, **41**:7892–7895.
18. Perdew JP, Burke K, Ernzerhof M: Generalized gradient approximation made simple. *Phys Rev Lett* 1996, **77**:3865.
19. Barbier A, Stierle A, Kasper N, Guittet M–J, Jupille J: Surface termination of hematite at environmental oxygen pressures: Experimental surface phase diagram. *Phys Rev B* 2007, **75**:233406.
20. Shivakumara C: Low temperature synthesis and characterization of rare earth orthoferrites LnFeO$_3$ (Ln=La, Pr and Nd) from molten NaOH flux. *Solid State Commun* 2006, **139**:165.
21. Lee CW, Behera RK, Wachsman ED, Phillpot SR, Sinnott SB: Stoichiometry of LaFeO3 (010) surface determined from first-principles and thermodynamic calculations. *Phys Rev B* 2011, **83**:115418.
22. Giraudon J–M, Elhachimi A, Wyrwalski F, Siffert S, Aboukais A, Lamonier J–F, Leclercq G: Studies of the activation process over Pd perovskite-type oxides used for catalytic oxidation of toluene. *Appl Catal B: Environmental* 2007, **75**:157.
23. Miquel P, Yamin Y, Lombaert K, Dujardin C, Granger P: Thermal ageing induced effects on Pd/LaFeO3 for NOx reduction by hydrocarbons: influence of the preparation method. *Top Catal* 2009, **52**:1791.
24. Humphrey W, Dalke A, Schulten K: VMD: visual molecular dynamics. *J Mol Graphics* 1996, **14**:33.
25. Monkhorst HJ, Pack JD: Special points for Brillouin-zone integrations. *Phys Rev B* 1976, **13**:5188.
26. Linstrom PJ: *Mallard WG (Eds): NIST Chemistry WebBook, NIST Standard Reference Database No. 69*. National Institute of Standards and Technology: Gaithersburg, MD; 2003.

doi:10.1186/1556-276X-8-203
Cite this article as: Tian *et al.*: First-principles investigation on the segregation of Pd at LaFe$_{1\text{-}x}$Pd$_x$O$_{3\text{-}y}$ surfaces. *Nanoscale Research Letters* 2013 **8**:203.